Chapter 3

New Approach to Mach-Zehnder Interferometer (MZI) Cell Based on Silicon Waveguides for Nanophotonic Circuits

Trung-Thanh Le

Additional information is available at the end of the chapter

http://dx.doi.org/10.5772/intechopen.76181

Abstract

In this chapter, we present a new scheme for Mach-Zehnder Interferometer (MZI) structure based on only one 4 × 4 multimode interference (MMI) coupler. We design the new MZI cell on the silicon on insulator (SOI) platform. The MZI based on directional coupler and 2 × 2 MMI coupler is also investigated in detail. The new MZI cell is a basic building block for photonic applications such as optical quantum gate, optical computing and reconfigurable processors. The numerical simulations show that our approach has advantages of compact size, ease of fabrication with the current complementary metal oxide semiconductor (CMOS) circuitry.

Keywords: multimode interference, silicon on insulator, multimode waveguide, directional coupler, finite difference time difference, finite difference method, modified effective index method

1. Introduction

Mach-Zehnder Interferometer (MZI) structure is a versatile component for photonic integrated circuits. A variety of photonic functional devices can be realized by using the MZI such as optical filter [1], add-drop multiplexer [2, 3], switch [4], modulator [5], sensor [6–8], tunable coupler [9, 10], signal transforms [11–13] and optical computing [14, 15], and so on.

In recent years, we have presented some approaches to realize optical signal processing based on MZI incorporated with microring resonators and multimode interference (MMI) coupler on a silicon on insulator (SOI) platform [16–20]. Silicon photonics is considered a key technology

for next generation optical interconnects, optical computing, data center and communication systems due to its low power operation, compactness, scalability and compatibility with the CMOS process. The SOI platform has a large index contrast between the silicon core and the silicon oxide/air cladding, thus allowing for small bend waveguides and denser integration of photonic components. Silicon photonic devices are also being considered for wavelength-division multiplexing (WDM) metro and long haul network segments.

It was shown that MZI is a basic element (basic cell) for optical photonic circuits and quantum technologies [21]. In [21], by cascading 15 MZIs with 30 thermo-optic phase shifters, a single programmable optical chip has been implemented. In [22], the author has presented a self-aligned universal beam coupler based on MZI elements that can take an arbitrary monochromatic input beam and, automatically and without any calculations, couple it into a single-mode guide or beam. This device can be used for special optical applications such as automatic compensation for misalignment and defocusing of an input beam, coupling of complex modes or multiple beams from fibers or free space to single-mode guides, and retaining coupling to a moving source. By using recursive algorithm, any discrete finite dimensional unitary operator based on MZI elements can also be constructed [23]. In addition, it was shown that optical neural networks based on architecture of 56 MZIs with 213 thermo-optic phase shifter elements have been implemented successfully [24]. This photonic circuit has been fabricated in an SOI platform with OpSIS (University of Washington's Optoelectronic Systems Integration in Silicon) foundry. An optical neuromorphic computing on a vowel recognition dataset has been demonstrated experimentally.

Very recently, universal multiport photonic interferometers by means of arrangements of reconfigurable MZIs on SOI platform can implement any arbitrary unitary transformation between input and output optical modes [25]. These arbitrary transforms are essential to support advanced optical functions such as linear quantum optical gates and circuits, microwave photonics signal processors, spatial mode converters, data center connections and optical networking functionalities. The triangle, square arrangements of MZI elements for hardware architecture are similar to the design principles of the field programmable gate arrays (FPGAs) in electronics. The core concept is to use a large network of identical two-dimensional unit or lattice cells implemented by means of MZIs. With a proper MZI element lattice arrangement, the architecture can implement a variety of functional configurations by mapping the desired matrix to a selection of signal paths through the architecture. By introducing the phase shifter elements in two arms of the MZI, a reconfigurable architecture can be implemented.

In the literature, the MZI consists of two 3 dB 2×2 directional couplers or 2×2 MMI couplers linked though two waveguide arms. It was shown that directional coupler is very sensitive to the fabrication error [16]. The power coupling ratios can be controlled by adjusting the coupling length and/or the gap between the two waveguides of the directional coupler [16]. In practice, accurate fabrication of the gap requires very tight control of the fabrication process. Moreover, additional loss due to mode conversion loss has been found to be a problem [26]. In contrast, MMI-based devices often have large fabrication tolerance, wide operation bandwidth and compact size. As a result, it is attractive to realize new functional devices based on MMIs for photonic applications.

In this chapter, we present a new MZI element architecture based on only one 4×4 MMI coupler on an SOI platform. The phase shifter based on a PN junction, which use the plasma

dispersion effect in silicon waveguides, is used. Our approach has advantages of compact size, ease of fabrication with the current CMOS circuit.

2. MZI cell based on directional couplers

2.1. Directional coupler type I

Figure 1 shows a general configuration of an MZI element based on two-directional couplers type I. Two arms of the MZI use two phase shifters with phase shifts ϕ_1 and ϕ_2. In our study, we use the PN junction operated in reverse bias, the depletion region is widened which lowers the overlap of the optical mode with charge carriers [5, 27]. As a result, the optical loss is low

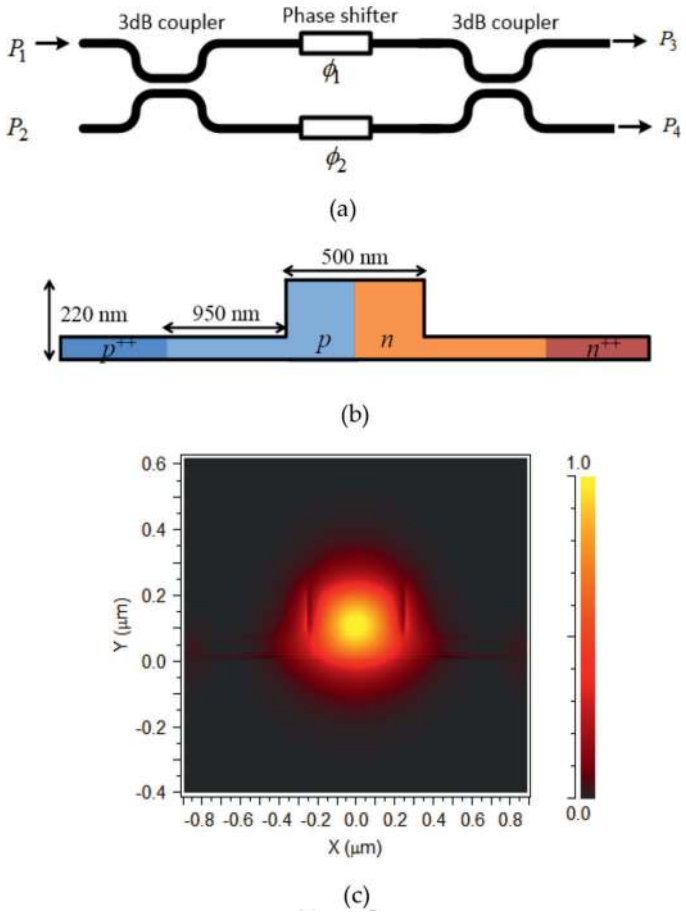

Figure 1. MZI cell based on directional coupler type I.

and the real part of the phase can be significantly increased compared with the forward bias. The change in index of refraction is phenomenologically described by Soref and Bennett model [28]. Here we focus on the central operating wavelength of around 1550 nm.

The change in refractive index Δn is described by:

$$\Delta n \text{ (at 1550 nm)} = -8.8 \times 10^{-22}\Delta N - 8.5 \times 10^{-18}\Delta P^{0.8} \quad (1)$$

The change in absorption $\Delta\alpha$ is described by:

$$\Delta\alpha \text{ (at 1550 nm)} = 8.5 \times 10^{-18}\Delta N + 6 \times 10^{-18}\Delta P \left[\text{cm}^{-1}\right] \quad (2)$$

where ΔN and ΔP are the free carriers concentrations of electrons and holes, respectively.

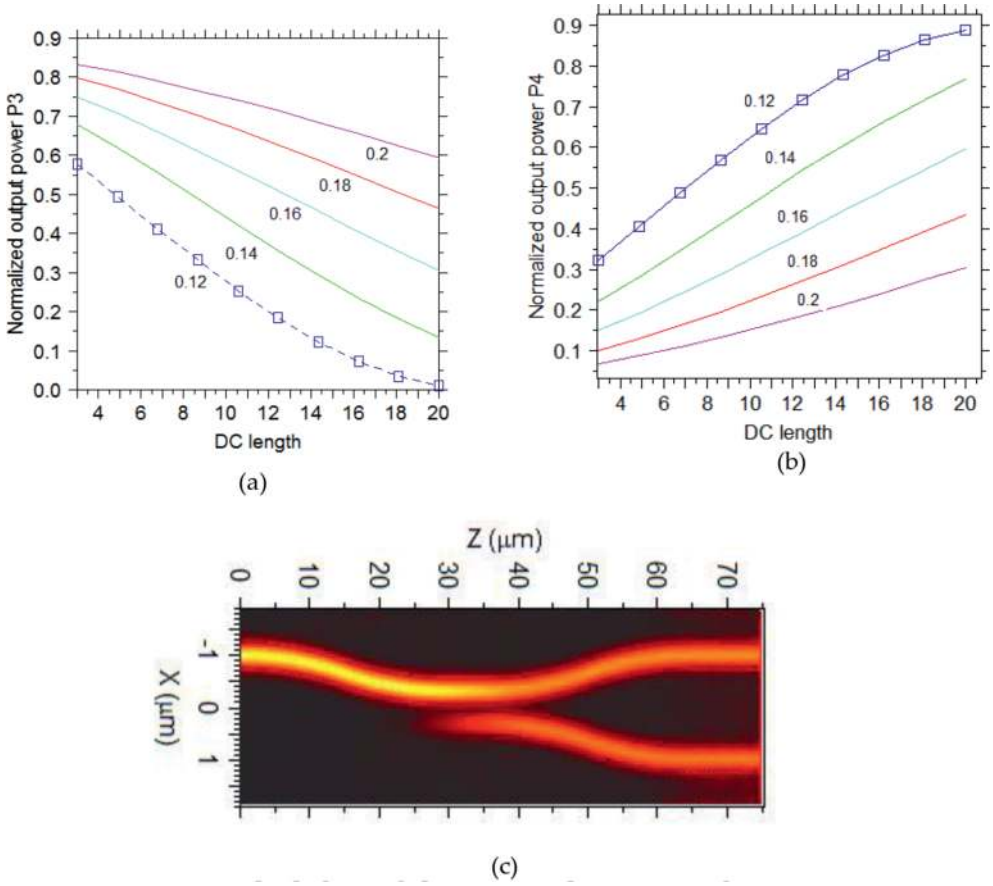

Figure 2. (a), (b) directional coupler design, type I for different separation between two waveguides g = 120, 140, 160, 180 and 200 nm and (c) field propagation at optimal length.

http://dx.doi.org/10.5772/intechopen.76181

The directional coupler can be characterized by a matrix [29]:

$$M_{DC} = \begin{pmatrix} t & jr \\ jr & t \end{pmatrix} \tag{3}$$

where t and r are the transmission and coupling coefficients of the coupler. The transfer matrix method is used to analyze the working principle of an MZI element. The relationship matrix between the input and output fields of the MZI can be expressed as [30].

$$\mathbf{S} = \begin{bmatrix} t & jr \\ jr & t \end{bmatrix} \begin{bmatrix} e^{j\phi_1} & 0 \\ 0 & e^{j\phi_2} \end{bmatrix} \begin{bmatrix} t & jr \\ jr & t \end{bmatrix} = \begin{pmatrix} t^2 e^{j\phi_1} - r^2 e^{j\phi_2} & jrt\left(e^{j\phi_1} + e^{j\phi_2}\right) \\ jrt\left(e^{j\phi_1} + e^{j\phi_2}\right) & t^2 e^{j\phi_2} - r^2 e^{j\phi_1} \end{pmatrix} \tag{4}$$

where t and r are optical field transmission and cross-coupling coefficients, respectively. For a 3 dB coupler, $r = t = 0.707$ [6, 13], the transfer matrix of the MZI is expressed by:

$$\mathbf{S} = je^{j\frac{\Delta\phi}{2}} \begin{bmatrix} \sin\dfrac{\Delta\phi}{2} & \cos\dfrac{\Delta\phi}{2} \\ \cos\dfrac{\Delta\phi}{2} & -\sin\dfrac{\Delta\phi}{2} \end{bmatrix} \tag{5}$$

where $\Delta\phi = \phi_1 - \phi_2$ is the phase shift difference between two arms.

A type I directional coupler is shown in **Figure 1**. This coupler consists of two adjacent waveguides with sine shapes separated by a coupler gap g. The normalized output powers or t^2, r^2 at different directional coupler (DC) length for coupler gap g = 120, 140, 160, 180 and 200 nm are shown in **Figure 2**. From these simulation results, we can achieve the optimal length of the directional coupler for 50:50 coupling ratio or 3 dB coupler. **Figure 2(c)** shows a field propagation for a 3 dB coupler with g = 120 nm and optimal length of 5 μm.

2.2. Directional coupler type II

An MZI cell based on a type II directional coupler is shown in **Figure 3**. The coupler consists of two adjacent waveguides with sine shape and rectangular shape separated by a coupler gap g. The normalized output powers or t^2, r^2 at different directional coupler (DC) length for coupler gap g = 120, 140, 160, 180 and 200 nm are shown in **Figure 4**. From these simulation results, we can achieve the optimal length of the directional coupler for 50:50 coupling ratio or 3 dB coupler. **Figure 4(c)** shows a field propagation for a 3 dB coupler with g = 120 nm and optimal length of 2μm.

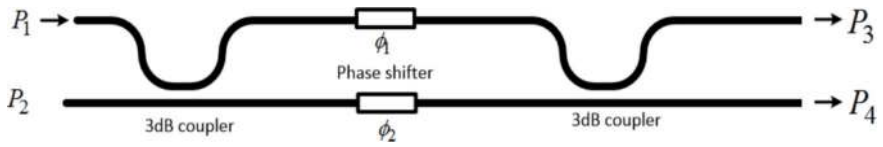

Figure 3. MZI cell based on directional coupler type II.

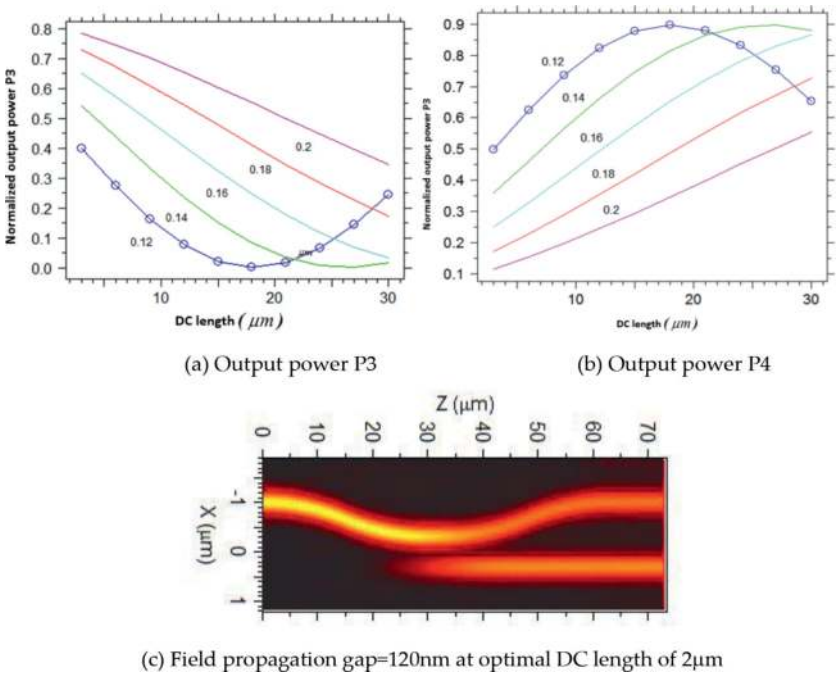

Figure 4. (a), (b) directional coupler design, type II for different separation between two waveguides g = 120, 140, 160, 180 and 200 nm and (c) field propagation at optimal length.

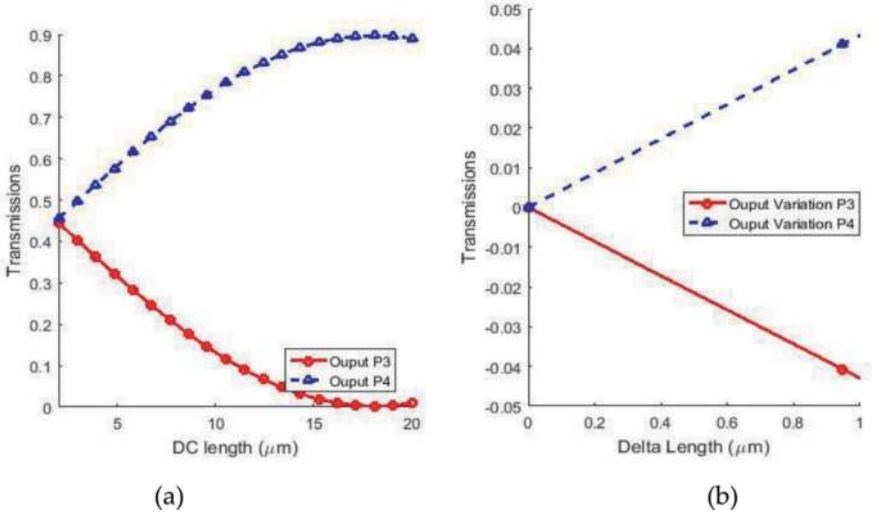

Figure 5. Transmissions of the directional coupler type II at different DC length.

http://dx.doi.org/10.5772/intechopen.76181

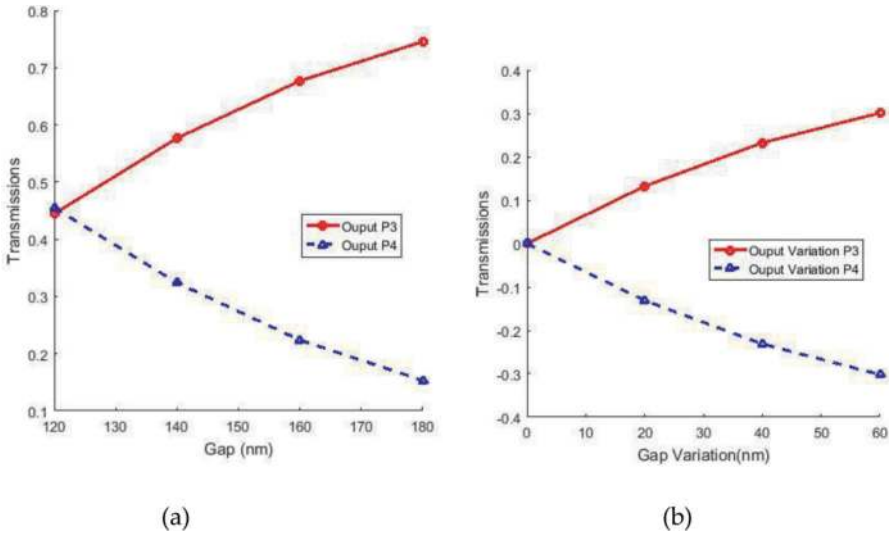

Figure 6. Transmissions of the directional coupler type II at different gap separation.

2.3. Fabrication tolerance analysis

Without loss of generality, we consider the directional coupler type II at the gap separation g = 120 nm for fabrication tolerance analysis. The fabrication tolerance of the directional coupler type I is similar to type II. The normalized output powers at the outputs are shown in **Figure 5**. We can see that a variation in length of ±100 nm results in a variation of 0.01 in normalized output powers. A change in a gap separation of ±10 nm will result in a change of 0.2 in normalized output power. As a result, the directional coupler type II is particularly sensitive to the fabrication error (**Figure 6**).

3. MZI cell based on 2 × 2 multimode interference coupler

The operation of an MMI coupler is based on the self-imaging principle or Talbot effect [31, 32]. The self-imaging shows that an input field is reproduced in single or multiple images at periodic intervals along the propagation direction of the MMI waveguide. The multimode waveguide is large enough to support a large number of modes.

There are two ways to create a 3 dB coupler based on MMI principle [20]: the first is the general interference (GI) mechanism which is independent of the modal excitation (we call MMI coupler type I in this chapter). The second is the restricted interference (RI) mechanism (MMI type II), in which excitation inputs are placed at some special positions so that certain modes are not excited.

3.1. MMI coupler type I

The MZI cell based on MMI couplers type I (GI-MMI) is shown in **Figure 7**. The MZI consists of two 3 dB MMI coupler. We have shown for the first time that a 3 dB GI-MMI coupler at the length of $1.5L_\pi$, where $L_\pi$is the beat length of the MMI coupler, can be expressed by a matrix [16]:

$$\mathbf{M}_{MMI,\,TypeI} = \frac{e^{j\phi_{GI}}}{\sqrt{2}}\begin{pmatrix} 1 & -j \\ -j & 1 \end{pmatrix} \tag{6}$$

where $\phi_{GI}$is a constant phase of the coupler.

$$\mathbf{S} = \frac{e^{j\phi_{GI}}}{\sqrt{2}}\begin{pmatrix} 1 & -j \\ -j & 1 \end{pmatrix}\begin{pmatrix} e^{j\phi_1} & 0 \\ 0 & e^{j\phi_2} \end{pmatrix}\frac{e^{j\phi_{GI}}}{\sqrt{2}}\begin{pmatrix} 1 & -j \\ -j & 1 \end{pmatrix} = je^{j2\phi_{GI}}e^{j\frac{\Delta\varphi}{2}}\begin{pmatrix} \sin\dfrac{\Delta\varphi}{2} & \cos\dfrac{\Delta\varphi}{2} \\ \cos\dfrac{\Delta\varphi}{2} & -\sin\dfrac{\Delta\varphi}{2} \end{pmatrix} \tag{7}$$

The first step is to optimize the MMI sections: we use tapered waveguides with a length of 3 μm for access waveguides in order to improve the device performance. The multimode sections need to be wide enough to achieve good performance and to be spaced apart sufficiently to limit crosstalk between the adjacent access waveguides. By using the numerical simulations, we choose the width of the MMI waveguide is 3 μm. The three-dimensional beam propagation method (3D-BPM) is used to carry out the simulations for the device having a length of 52.2 μm. The aim of this step is to find roughly the positions which result in a power splitting of 50/50, that is, a 3 dB coupler. Then, the 3D-BPM is used to perform the simulations around these positions to locate the best lengths. The normalized output powers of the 2 × 2 GI-MMI coupler at different lengths of the couplers are plotted in **Figure 8**. The field propagations at the optimal length through the 3 dB GI-MMI coupler and the MZI cell are shown in

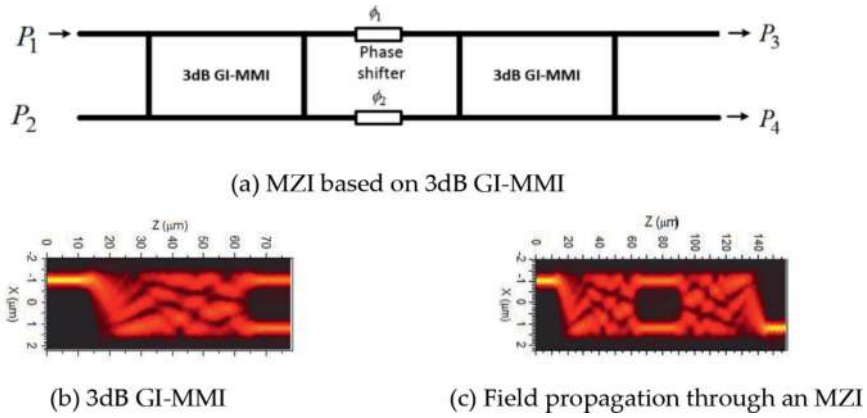

Figure 7. MZI cell based on 3 dB MMI type I.

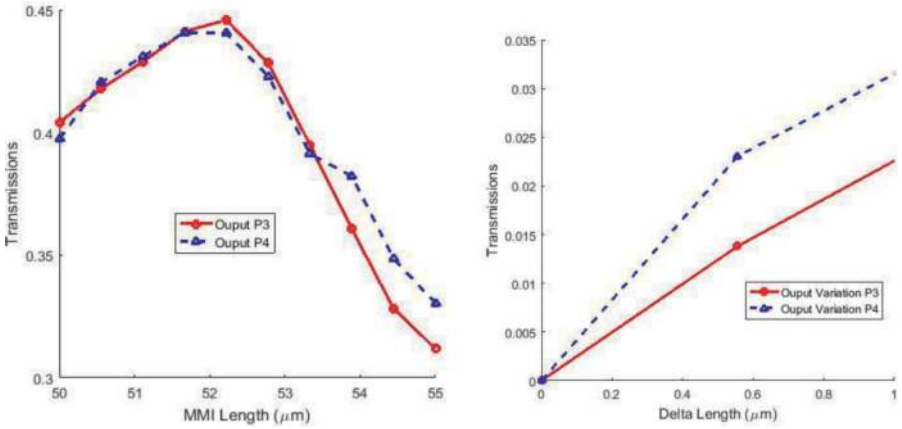

Figure 8. MZI cell based on 3 dB MMI type I.

Figure 7(b) and **(c)**. The simulations show that a variation in MMI length of ±100 nm will result in a change of 0.005 in normalized powers as shown in **Figure 8(b)**. Therefore, the MMI coupler has a much large fabrication tolerance compared with the directional coupler.

3.2. MMI coupler type II

The MZI cell based on MMI couplers type II (RI-MMI) is shown in **Figure 9**. We have shown that a 3 dB RI-MMI coupler at the length of $0.5L_\pi$, where $L_\pi$is the beat length of the MMI coupler, can be expressed by a matrix [16]:

$$\mathbf{M}_{MMI,\,TypeII} = \frac{e^{j\phi_{RI}}}{\sqrt{2}}\begin{pmatrix} 1 & j \\ j & 1 \end{pmatrix} \tag{8}$$

where $\phi_{RI}$is a constant phase of the coupler.

$$\mathbf{S} = \frac{e^{j\phi_{RI}}}{\sqrt{2}}\begin{pmatrix} 1 & j \\ j & 1 \end{pmatrix}\begin{pmatrix} e^{j\phi_1} & 0 \\ 0 & e^{j\phi_2} \end{pmatrix}\frac{e^{j\phi_{RI}}}{\sqrt{2}}\begin{pmatrix} 1 & j \\ j & 1 \end{pmatrix} = je^{j2\phi_{RI}}e^{j\frac{\Delta\varphi}{2}}\begin{pmatrix} \sin\dfrac{\Delta\varphi}{2} & \cos\dfrac{\Delta\varphi}{2} \\ \cos\dfrac{\Delta\varphi}{2} & -\sin\dfrac{\Delta\varphi}{2} \end{pmatrix} \tag{9}$$

By using the numerical simulations, we choose the width of the MMI waveguide is 4 μm. The 3D-BPM is used to carry out the simulations for the device having a length of 33.4 μm. The normalized output powers of the 2 × 2 RI-MMI coupler at different lengths of the couplers are plotted in **Figure 10(a)**. The field propagations at the optimal length through the 3 dB RI-MMI coupler and the MZI cell are shown in **Figure 9(b)** and **(c)**. The simulations show that a variation in MMI length of ±100 nm will result in a change of 0.005 in normalized powers as shown in **Figure 10(b)**.

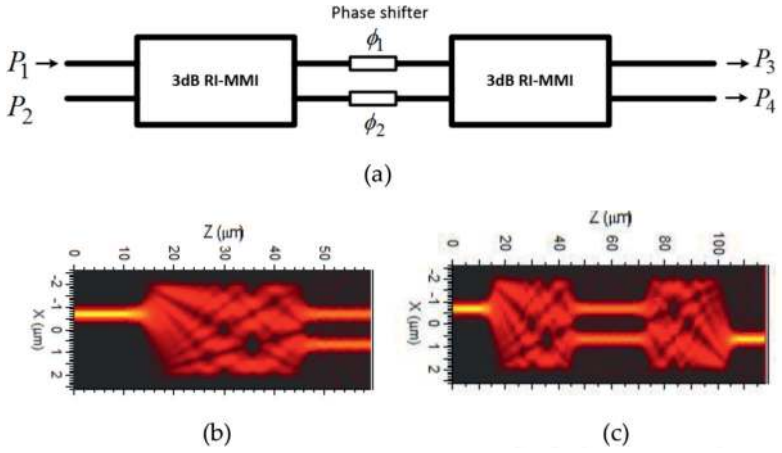

Figure 9. MZI cell based on 3 dB MMI type II.

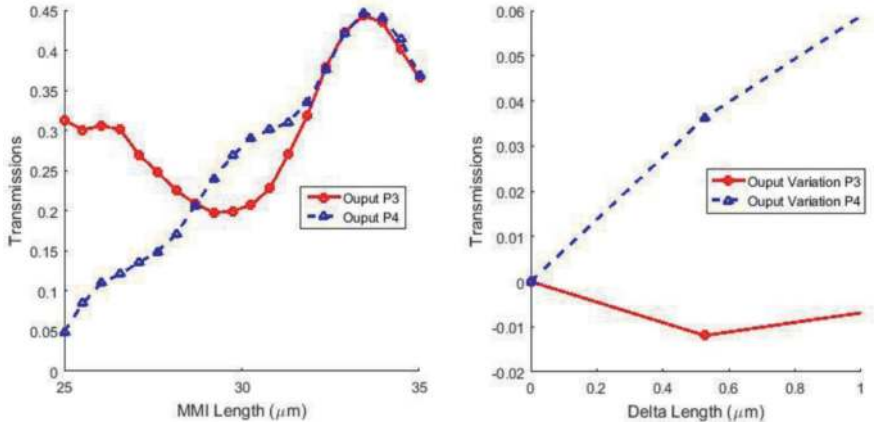

Figure 10. MZI cell based on 3 dB MMI type II.

4. MZI cell based on a 4 × 4 MMI coupler

Figure 11 shows the new scheme of our new proposed MZI cell based on only one 4 × 4 MMI coupler. We choose the width of the 4 × 4 MMI coupler is 6 μm. The optimal length of the MMI is calculated by the 3D-BPM [33]. We show that the optimal length is found to be 115.8 μm. **Figure 11(b)** and **(c)** shows the field propagation through the 4 × 4 MMI coupler at the optimal length for input signal at port 1 and port 2, respectively.

Figure 12 shows the normalized output powers at output port 1 and 4 while the input signal is at input port 1.

http://dx.doi.org/10.5772/intechopen.76181

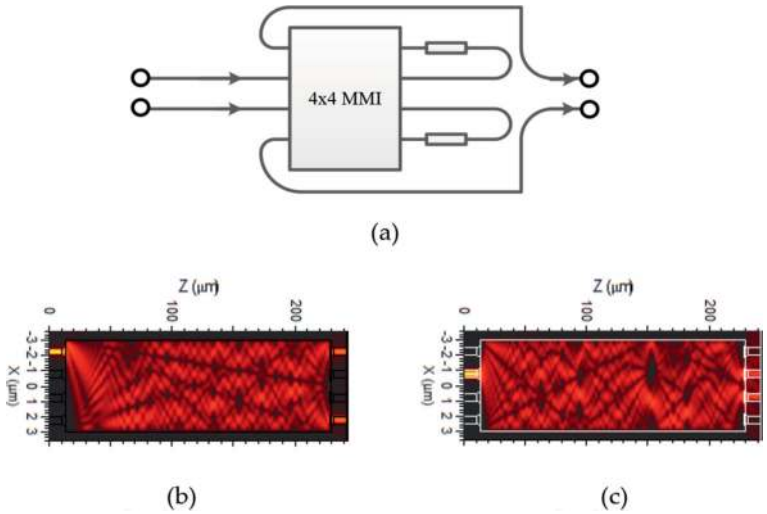

Figure 11. MZI cell based on 4 × 4 MMI coupler.

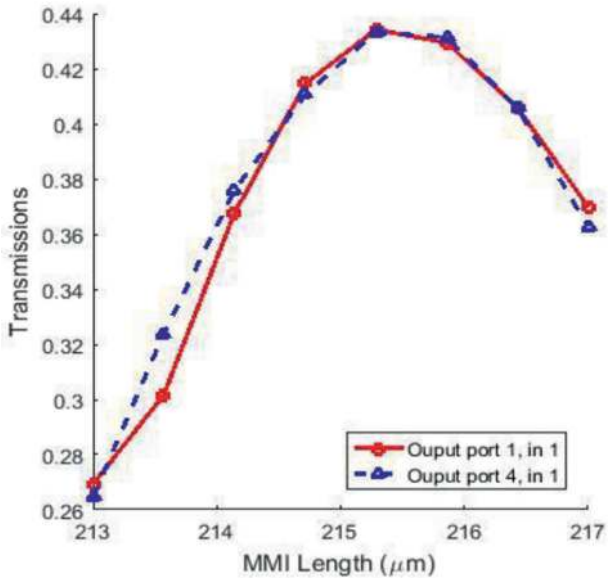

Figure 12. Normalized output powers at output port 1 and 4 of a 4 × 4 MMI coupler.

By some calculations, the MZI cell based on 4 × 4 MMI coupler can be expressed by a characterized matrix

$$\mathbf{S} = \frac{1}{\sqrt{2}}\begin{bmatrix} 1 & j \\ j & 1 \end{bmatrix}\begin{bmatrix} e^{j\Delta\varphi} & 0 \\ 0 & 1 \end{bmatrix}\frac{1}{\sqrt{2}}\begin{bmatrix} 1 & j \\ j & 1 \end{bmatrix} = e^{j\frac{\Delta\varphi}{2}}\begin{bmatrix} \tau & \kappa \\ \kappa^* & -\tau^* \end{bmatrix} \tag{10}$$

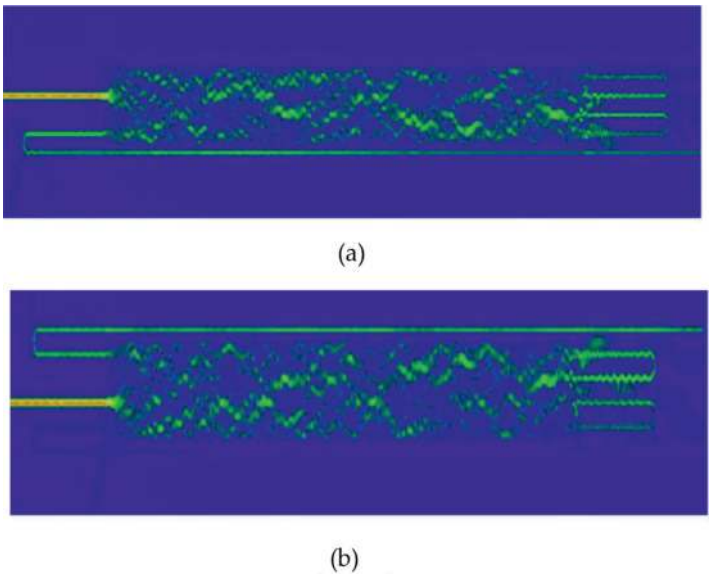

Figure 13. Optical field propagation through the coupler for input signal presented at port 2 and 3.

where $\tau = \sin\left(\frac{\Delta\varphi}{2}\right)$, and $\kappa = \cos\left(\frac{\Delta\varphi}{2}\right)$.

Finally, we use finite difference time difference (FDTD) method to simulate the proposed MZI cell and then make a comparison with the analytical theory. The proposed MZI cell has two feedback waveguides. Although the BPM has an advantage of fast simulations and it is widely used technique to simulate light propagation in slowly varying non-uniform guiding structures, it is not suitable for simulating the proposed MZI structure. The FDTD has a disadvantage of a time-consuming simulation, and it has very accurate results. In our FDTD simulations, we take into account the wavelength dispersion of the silicon waveguide. A light pulse of 15 fs pulse width is launched from the input to investigate the transmission characteristics of the device. The grid sizes $\Delta x=\Delta y=\Delta z = 20$ nm are chosen in our simulations for accurate simulations [34]. The FDTD simulations for the MZI cell are shown in **Figure 13**. The simulations show that the device operation has a good agreement with our prediction by analytical theory.

5. Waveguide mesh design with new MZI cell

The new proposed MZI cell is a basic building block for mesh design to produce new functional devices for photonic applications. For example, by using the hexagonal mesh shown in

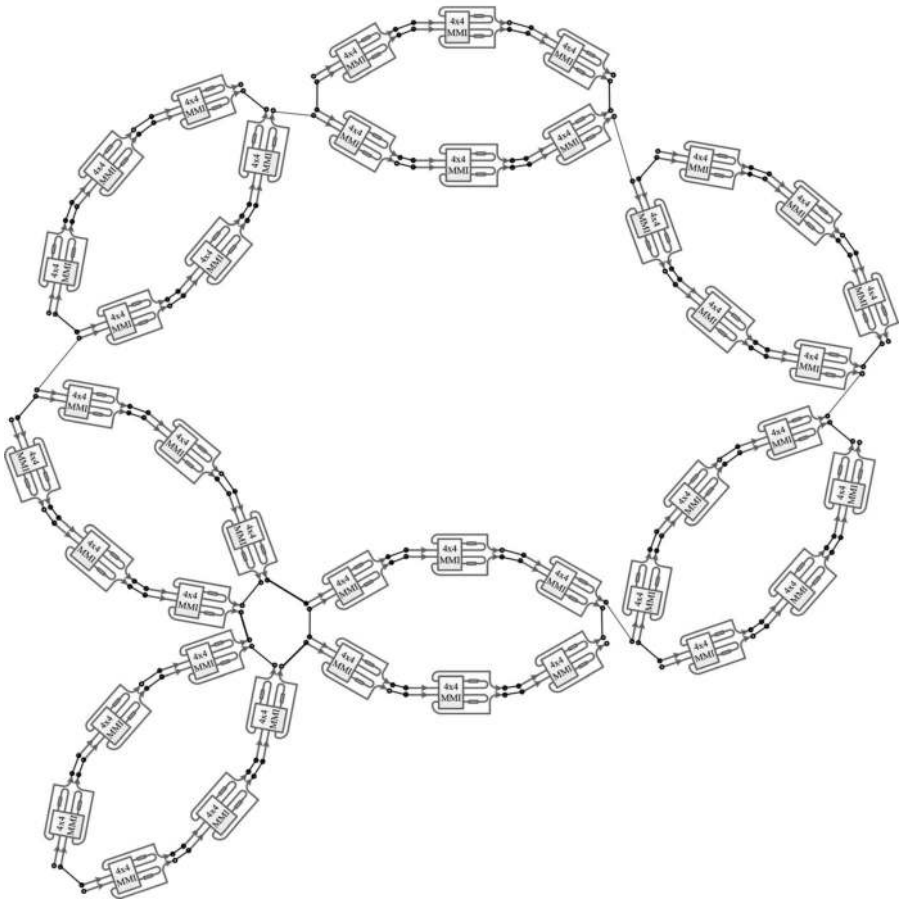

Figure 14. Reconfigurable mesh design based on new MZI cell.

Figure 14, optical filters and switches can be achieved by properly controlling the phase shifters.

6. Conclusions

We presented a new compact MZI cell based on silicon on insulator waveguides. The structure requires only one 4×4 multimode interference coupler. The PN junction waveguide is used to achieve reconfigurable devices. The device operation has been verified by using the FDTD. This MZI cell can be useful for complex mesh designs applied to optical applications.

Author details

Trung-Thanh Le

Address all correspondence to: thanh.le@vnu.edu.vn

International School (VNU-IS), Vietnam National University (VNU), Hanoi, Vietnam

References

[1] Agrawal GP. Fiber Optic Communication Systems. New York: John Wiley & Sons; 2002

[2] Le T-T, Cahill L. Microresonators based on 3 × 3 restricted interference MMI couplers on an SOI platform. In: IEEE LEOS Annual Meeting Conference Proceedings (LEOS 2009). Belek-Antalya, Turkey; October 4–8, 2009. pp. 479-480

[3] Le T-T, Cahill L. The design of 4 × 4 multimode interference coupler based microring resonators on an SOI platform. Journal of Telecommunications and Information Technology. 2009;**2**:98-102

[4] Le TT, Cahill LW. The design of wavelength selective switches and filters based on SOI microring resonators. In: 2007 Asia-Pacific Conference on Communications; 2007. pp. 3-5

[5] Le D-T, Nguyen N-M, Le T-T. Development of PAM-4 signaling for high performance computing, supercomputers and data center systems. Journal of Science and Technology on Information and Communications. 2017;**1**:34-38

[6] Le T-T. Realization of a multichannel chemical and biological sensor using 6 × 6 multimode interference structures. International Journal of Information and Electronics Engineering. 2011;**2**:240-244

[7] Le T-T. Microring resonator based on 3 × 3 general multimode interference structures using silicon waveguides for highly sensitive sensing and optical communication applications. International Journal of Applied Science and Engineering. 2013;**11**:31-39

[8] Le T-T. Two-channel highly sensitive sensors based on 4 × 4 multimode interference couplers. Photonic Sensors. 2017;**7**:357-364, 2017/12/01

[9] Le TT, Cahill LW, Elton DM. Design of 2 × 2 SOI MMI couplers with arbitrary power coupling ratios. Electronics Letters. 2009;**45**:1118-1119

[10] Le T-T. Arbitrary power splitting couplers based on 3 × 3 multimode interference structures for all-optical computing. International Journal of Engineering and Technology. 2011;**2**:565-569

[11] Le T-T. Realization of all-optical type i discrete cosine and sine transforms using multimode interference structures. International Journal of Microwave and Optical Technology (IJMOT). 2012;**7**:127-134

[12] Le T-T. All-optical Karhunen–Loeve transform using multimode interference structures on silicon nanowires. Journal of Optical Communications. 2011;**32**:217-220

[13] Le T-T. The design of optical signal transforms based on planar waveguides on a silicon on insulator platform. International Journal of Engineering and Technology. 2010;**2**:245-251

[14] Le T-T. Arbitrary power splitting couplers based on 3 × 3 multimode interference structures for all-optical computing. International Journal of Engineering and Technology. 2011;**3**:565-569

[15] Le D-T, Le T-T. Coupled resonator induced transparency (CRIT) based on interference effect in 4 × 4 MMI coupler. International Journal of Computer Systems (IJCS). 2017;**4**:95-98

[16] Le T-T. Multimode Interference Structures for Photonic Signal Processing. Germany: LAP Lambert Academic Publishing; 2010

[17] Cahill LW, Le TT. MMI devices for photonic signal processing. In: 9th International Conference on Transparent Optical Networks (ICTON 2007). Rome, Italy; July 1–5, 2007. pp. 202-205

[18] Cahill LW, Le TT. Photonic signal processing using MMI elements. In: 10th International Conference on Transparent Optical Networks (ICTON 2008); Athens, Greece; 22-26 June 2008. pp.114-117

[19] Le TT, Cahill LW. The modeling of MMI structures for signal processing applications. In: Greiner CM, Waechter CA, editors. Integrated Optics: Devices, Materials, and Technologies XII. Proceedings of the SPIE. Vol. 6896. San Jose, California, United States: Society of Photo-Optical Instrumentation Engineers (SPIE); pp. 68961G-68961G-7, 03/2008

[20] Le TT, Cahill L. All-optical signal processing circuits using silicon waveguides. In: The 7th International Conference on Broadband Communications and Biomedical Applications. Melbourne, Australia; ; November 21–24, 2011. pp. 167-172

[21] Carolan J, Harrold C, Sparrow C, et al. Universal linear optics. Science. 2015;**349**:711

[22] Miller DAB. Self-aligning universal beam coupler. Optics Express. 2013;**21**:6360-6370

[23] Reck M, Zeilinger A, Bernstein HJ, et al. Experimental realization of any discrete unitary operator. Physical Review Letters. 1994;**73**:58-61

[24] Shen Y, Harris NC, Skirlo S, et al. Deep learning with coherent nanophotonic circuits. Nature Photonics. 2017;**11**:441

[25] Perez D, Gasulla I, Fraile FJ, et al. Silicon photonics rectangular universal interferometer. Laser & Photonics Reviews. 2017;**11**:1700219

[26] Xia F, Sekaric L, Vlasov YA. Mode conversion losses in silicon-on-insulator photonic wire based racetrack resonators. Optics Express. 2006;**14**:3872-3886

[27] Baehr-Jones T, Ding R, Liu Y, et al. Ultralow drive voltage silicon traveling-wave modulator. Optics Express. 2012;**20**:12014-12020

[28] Emelett SJ, Soref R. Design and simulation of silicon microring optical routing switches. IEEE Journal of Lightwave Technology. 2005;**23**:1800-1808

[29] Heebner J, Grover R, Ibrahim T. Optical Microresonators: Theory, Fabrication, and Applications. London: Springer; 2008

[30] Le T-T, Cahill L. Generation of two Fano resonances using 4 × 4 multimode interference structures on silicon waveguides. Optics Communications. 2013;**301-302**:100-105

[31] Bachmann M, Besse PA, Melchior H. General self-imaging properties in N × N multimode interference couplers including phase relations. Applied Optics. 1994;**33**:3905

[32] Soldano LB, Pennings ECM. Optical multi-mode interference devices based on self-imaging: Principles and applications. IEEE Journal of Lightwave Technology. 1995;**13**:615-627

[33] Le T-T. An improved effective index method for planar multimode waveguide design on an silicon-on-insulator (SOI) platform. Optica Applicata. 2013;**43**:271-277

[34] Le D-T, Nguyen M-C, Le T-T. Fast and slow light enhancement using cascaded microring resonators with the Sagnac reflector. Optik – International Journal for Light and Electron Optics. 2017;**131**:292-301